

Direction-Controllable Electromagnetic Acoustic Transducer for SH Waves in Steel Plate Based on Magnetostriction

Yu Zhang, Song Ling Huang*, Shen Wang, and Wei Zhao

Abstract—Shear-horizontal (SH) wave is commonly used in monitoring and detecting steel plate structures. Electromagnetic acoustic transducer (EMAT) based on magnetostriction owns higher transducing efficiency and can be applied in non-contact situations. In some practical applications, it is necessary to inspect the structure on a specific direction and the inspecting direction is required to be variable and accurately controllable. This work proposes a novel direction-controllable EMAT for SH0 mode waves based on magnetostriction. Theoretical foundation and analysis on the magnetostriction model of the new EMAT and working parameters determination are conducted. The detailed structure and design of the new EMAT are presented, with the pre-magnetized open annular nickel strap bonded to the steel plate providing the circumferential static bias magnetic field, and the cooperation of embedded conductors in the rotating slider and open metal rings providing the dynamic magnetic field. Besides, the experimental system for the performance verification of the new EMAT is setup. Three indexes, the dead zone angle, focus angle and consistency error are defined to evaluate the performance quantitatively. The dead zone angle of the new EMAT is 28.74° ; the focus angle is 10.7° ; the consistency error is only 1.4%. Experimental results show that the proposed direction-controllable EMAT is highly directional. The stimulating direction can be accurately controlled, and the circumferential consistency is fairly high. The direction-controllable EMAT can hopefully provide a practical solution for directional monitoring and inspecting for steel plate structures.

1. INTRODUCTION

Non-destructive testing and evaluation play a significant role in monitoring and inspecting the safety and integrity of structural components [1, 2]. On account of prominent properties on large-area scanning, ultrasonic guided wave (GW) has been importantly applied in the fast inspection for metal structures such as industrial plates and pipes in recent years [3–6]. Shear-horizontal (SH) wave is one of the commonly used types of GW with the advantage of being free of mode conversion during the propagation and when reflection occurs at the medium interface [7]. The multi-modes characteristics and dispersion phenomenon of GW can make it really complex to analyze the detection signals of defects [8, 9]. But SH0 mode GW is free of dispersion, and the group velocity is a constant for the given materials and parameters of the structure, instead of varying with the working frequency [10]. This feature of SH0 mode GW lays the theoretical foundation for accurate detection of defects by SH0 mode wave [11].

Piezoelectric transducers are commonly used for transmitting and receiving GW [12, 13]. But liquid couplant is needed for the transduction process in piezoelectric transducers, and this confines their application in some non-contact and high temperature situations [14]. Electromagnetic acoustic transducer (EMAT) has been developed recently to overcome the above shortcomings by electromagnetic coupling, with advantages of being able to control the modes of stimulated GW by different designs

Received 22 July 2016, Accepted 7 September 2016, Scheduled 29 September 2016

* Corresponding author: Song Ling Huang (huangsling@tsinghua.edu.cn).

The authors are with the State Key Laboratory of Power Systems, Department of Electrical Engineering, Tsinghua University, Beijing 100084, China.

of bias magnetic fields and coils [15, 16]. Magnetostriction plays a dominant role in the transduction mechanism of EMAT for steel structures and owns relatively higher transducing efficiency compared with that based on Lorentz force [17].

Researches about EMAT or other types of transducers are mainly focused on the performance improvement [18, 19], including the directionality of the stimulated GW. Seung et al. proposed an omnidirectional SH wave EMAT using a pair of ring-type permanent magnets [20]. Wilcox et al. designed an omnidirectional EMAT array for the fast inspection of metallic plate [21]. An inner-digital transducer type Lamb wave sensor was proposed by Roh and Kim, which was more readily controllable than conventional piezoelectric sensors [22]. A type of annular transducer array was applied in Masuyama et al.'s work to generate a narrow beam with given radiation direction by numerical calculation [23]. In previously published papers, the directionalities of EMAT are mostly omnidirectional [24], but the detection along particular given direction can hardly be accurately controlled. However, in some practical situations, it is necessary to conduct GW testing on a specific direction of the structure, and the detecting direction is required to be variable and accurately controllable. This contradiction desiderates a practical and feasible solution to accurately control the direction of GW and cover almost all directions as sufficient as possible.

In this work, a novel direction-controllable EMAT for SH waves in steel plate based on magnetostriction is proposed. The theoretical foundation of SH waves and magnetostriction model of EMAT are analyzed. And the structure of the direction-controllable EMAT is demonstrated in detail. In order to evaluate the performance of the new EMAT quantitatively, three indexes which are the dead zone angle, focus angle and consistency error are defined and calculated. Besides, the experimental system for the performance verification was set up, and related experiments were conducted.

2. THEORETICAL ANALYSIS

In order to optimize the performance of the direction-controllable EMAT, the working points of SH waves and parameters of EMAT need to be firstly determined. Based on dispersion equations of GW [8], Fig. 1 illustrates the dispersion curves of SH waves for a 4 mm thick steel plate, in which the longitudinal wave velocity is configured as 5940 m/s, and the transverse wave velocity is configured as 3200 m/s.

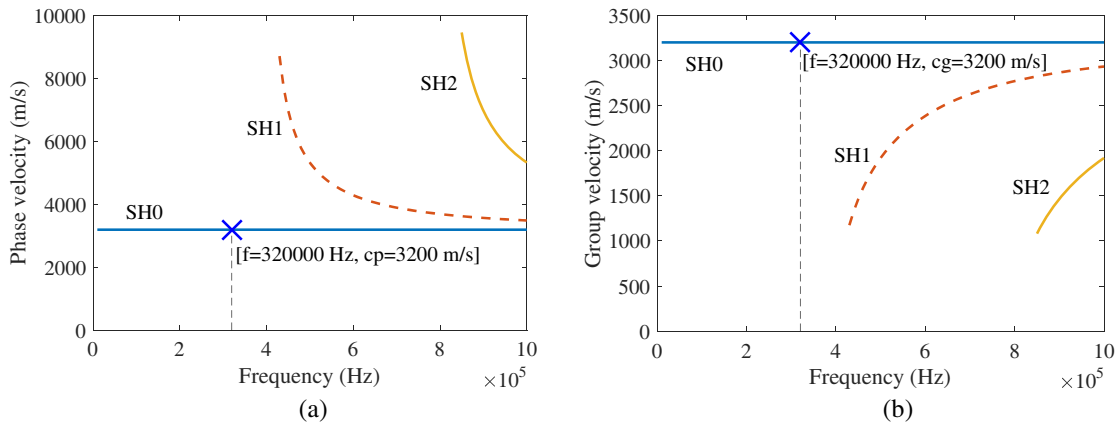


Figure 1. Dispersion curves of SH waves for a 4 mm thick steel plate, (a) phase velocity dispersion curves, (b) group velocity dispersion curves.

It can be indicated in Fig. 1 that neither the phase velocity nor the group velocity of SH0 mode wave changes with the working frequency. Instead, both of them remain a constant of 3200 m/s. And the working point is selected as 320 kHz, at which only SH0 mode wave exists, and this configuration can avoid the interference of multi-modes SH waves. Besides, for SH waves, mode conversion will not occur during the propagation process or at the interface of two different mediums. Therefore, SH0 mode wave at the working frequency 320 kHz is selected to inspect the 4 mm thick steel plate.

Magnetostriction usually takes a dominant role for stimulating GW in ferromagnetic materials, because of the higher transduction efficiency, especially in relatively weak magnetic situations [17]. The magnetostriction model for EMAT is illustrated in Fig. 2. And the EMAT is composed of three parts: the static bias magnetic field, coil with alternating current and ferromagnetic material being tested.

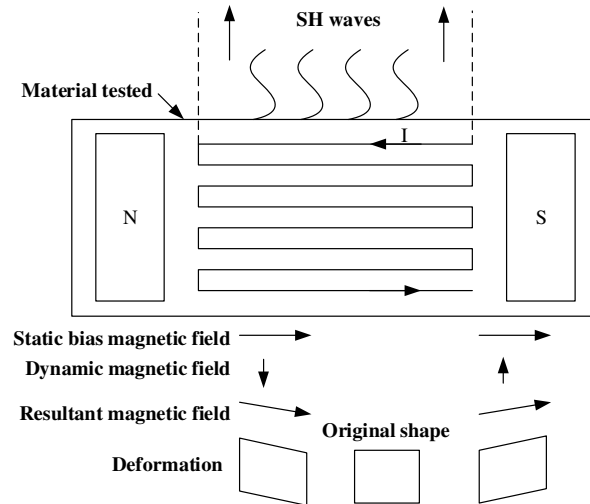


Figure 2. Schematic diagram of the magnetostriction model for EMAT.

In the magnetostriction model, the static bias magnetic field can be provided by a permanent magnet, an electromagnet or a kind of magnetic material that is pre-magnetized. The dynamic magnetic field is induced by the alternating current in the contra-flexure coil. And the static bias magnetic field is vertical to the dynamic magnetic field. The shape of the magnetic domain will be alternately deformed due to the alternately changing resultant magnetic field. The alternate deformation gives rise to the local vibration of the material being tested, and the GW is then stimulated. The GW will propagate along the direction that is vertical to the static bias magnetic field and be confined in the range of the width of the contra-flexure coil. The GW can be received based on the inverse magnetostriction.

3. THE DESIGN OF THE DIRECTION-CONTROLLABLE EMAT

Based on the working point of SH0 mode wave and the magnetostriction model for EMAT, the structure of the direction controllable EMAT is illustrated in Fig. 3. The shell of the direction controllable EMAT is in a cylindrical shape, and the direction rotary knob in the center of the top surface outside the shell is to accurately control the direction of the stimulated SH0 waves. The shaft is directly connected to the direction rotary knob, and it will rotate with the knob. The shaft is fixed in the vertical direction by bearings from the shell and the supporting, which is installed on the shell.

The rotating slider is installed on the shaft, and it will rotate along the circumferential direction with the shaft and keep pace with the direction rotary knob. A detailed view of the rotating slider part is illustrated in Fig. 3(b). There are some arc grooves on the bottom surface of the rotating slider, and they can fit well with the open metal rings, so that the rotating slider can rotate smoothly on the open metal rings. The open annular nickel strap is bonded on the surface of the steel plate being detected by epoxy resin adhesive. There is a layer of insulating coat between the open metal rings and open annular nickel strap, and the open metal rings are installed on the insulating coat. Some embedded conductors are inserted in the bottom surface of the rotating slider. The embedded conductors are electrically and reliably connected to some parts of the open metal rings that are below the rotating slider. The top view of the direction-controllable EMAT in Fig. 4 shows a clearer description.

The embedded conductors inserted in the rotating slider and the open metal rings that are electrically connected to the conductors make up the current coils for the new EMAT, represented

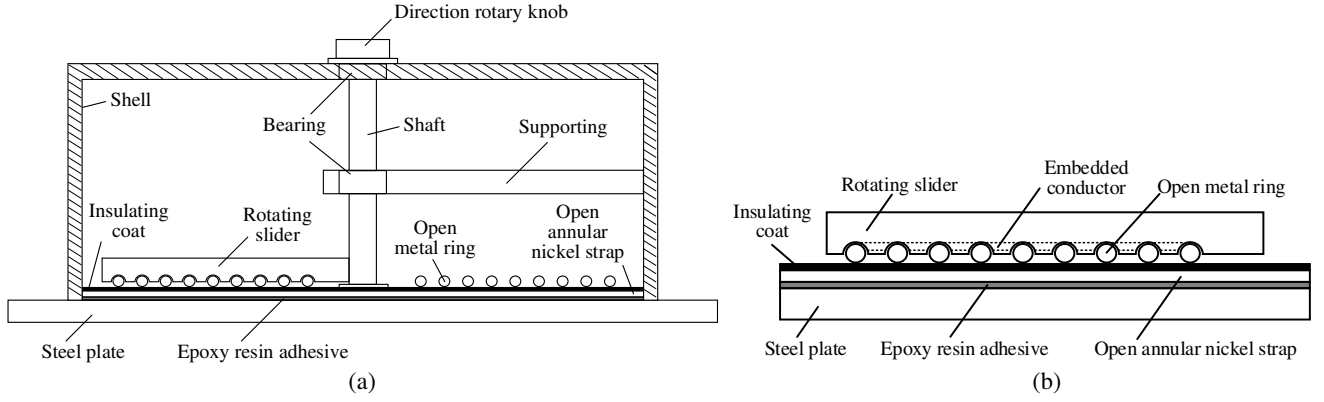


Figure 3. The structure of the direction-controllable EMAT, (a) front view of the new EMAT, (b) detailed view of the rotating slider part.

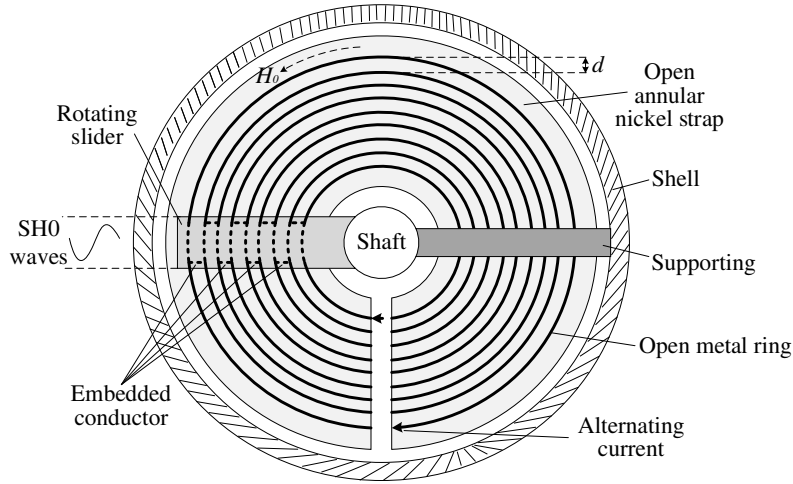


Figure 4. The top view of the direction-controllable EMAT.

by the dotted lines below the rotating slider shown in Fig. 4. And the current coils work in a similar way to the contra-flexure coils in the magnetostriction EMAT model in Fig. 2, being energized by the alternating current and providing the dynamic magnetic field. The static bias magnetic field H is in the circumferential direction, and it is provided by the remanence of the open annular nickel strap, which is previously magnetized in the circumferential direction. Based on the magnetostriction model, SH waves will be stimulated in the radial direction, and the majority of the SH waves energy will be confined in the range of the width of the rotating slider. Therefore, when the rotating slider rotates circumferentially on the open metal rings, SH waves can be stimulated at desired directions, and the propagating directions of SH waves can be accurately controlled by the direction rotary knob outside the shell.

Based on the working point selected in Fig. 1, the working frequency f of the new EMAT is 320 kHz, and the group velocity c of SH0 waves is 3200 m/s. The wavelength λ of SH0 waves can be calculated

$$\lambda = \frac{c}{f} \quad (1)$$

Therefore, the wavelength of the stimulated SH0 waves is 1 cm. In order to generate pure SH0 mode waves and enhance the amplitude of the SH0 waves, the distance d between any two adjacent open metal rings should be

$$d = \frac{\lambda}{2} = \frac{c}{2f} \quad (2)$$

The reason for this relationship is that the current phase difference in any two adjacent open metal rings is π , which is half cycle, so the phase difference of the dynamic magnetic fields is also half cycle. If the distance d is set as odd times of the half wavelength, the vibrations induced by these two SH waves have the same phase and will constantly reinforce each other, which can effectively enhance the amplitude of the generated SH0 waves [25]. So the distance d is set as 0.5 cm.

Because a radial gap exists between the two poles of the open annular nickel strap, there will be a circumferential angle range that the rotating slider cannot reach, which forms a direction dead zone for the direction-controllable EMAT. Fig. 5 describes the definition of the direction dead zone. When the lateral margin of the rotating slider reaches the margin of the gap, that is the boundary for the rotation range of the rotating slider.

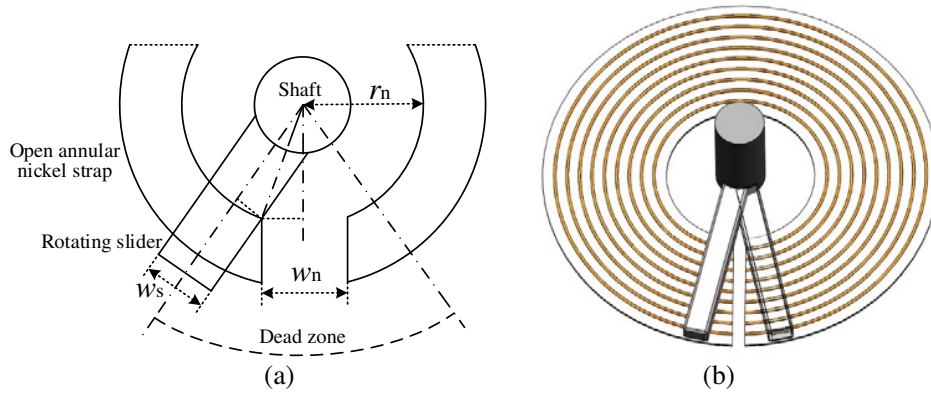


Figure 5. The direction dead zone of the direction-controllable EMAT. (a) Schematic illustration for the direction dead zone, (b) physical illustration for the direction dead zone.

In Fig. 5(a), the width of the rotating slider is w_s ; the width of radial gap of the open annular nickel strap is w_n ; the inside radius of the open annular nickel strap is r_n . According to their geometrical relationship, the dead zone angle θ_d can be calculated as

$$\theta_d = 2 \left(\arcsin \frac{\frac{w_s}{2}}{r_n} + \arcsin \frac{\frac{w_n}{2}}{r_n} \right) \quad (3)$$

For the direction-controllable EMAT in this work, the width of the rotating slider w_s is 1 cm; the width of radial gap of the open annular nickel strap w_n is 0.5 cm; the inside radius of the open annular nickel strap r_n is 3 cm, so the dead zone angle is about 28.74° . The dead zone angle is practically defined by the physical structure of the direction-controllable EMAT, where a radial gap exists between the two poles of the open annular nickel strap. The rotating slider should not cover the gap because it violates the magnetostriction model of the EMAT, and guided waves cannot be generated in this situation. The theoretical analysis or calculation, i.e., Equation (3), is almost totally based on the physical definition of the direction dead zone. Therefore, the calculation result of Equation (3) is practical and has clear physical meaning.

The outside diameter of the open annular nickel strap is 8 cm, so the width of the open annular nickel strap is 5 cm. The thickness of the open annular nickel strap is 0.5 mm, and the thickness of the insulating coat is 0.5 mm. There are nine open metal rings bonded on the surface of the insulating coat. The wire diameter of the open metal ring is 1 mm. So the lift-off distance from the center of the open metal ring to the center of the open annular nickel strap is 1.25 mm. The radius of the smallest open metal ring is 3.5 cm, and the radius of the largest open metal ring is 7.5 cm. In other words, the distance between the inner edge of the open annular nickel strap and the smallest open metal ring is 0.5 cm, and the distance between the outer edge of the open annular nickel strap and the largest open metal ring is also 0.5 cm. The height of the rotating slider is 7 mm, the height of the embedded conductor 0.5 mm, and the width of the embedded conductor 1 mm. The radius of the shaft is 1 cm, and the radius of the direction rotary knob is 6 cm.

4. EXPERIMENTS ABOUT THE PERFORMANCE OF THE NEW EMAT

Circumferential consistency, directionality and its focus level are important performance indexes for the direction-controllable EMAT. Some experiments will be conducted in this part to verify the superiority of the related indexes. Fig. 6 shows the schematic diagram and a photo of the experimental system.

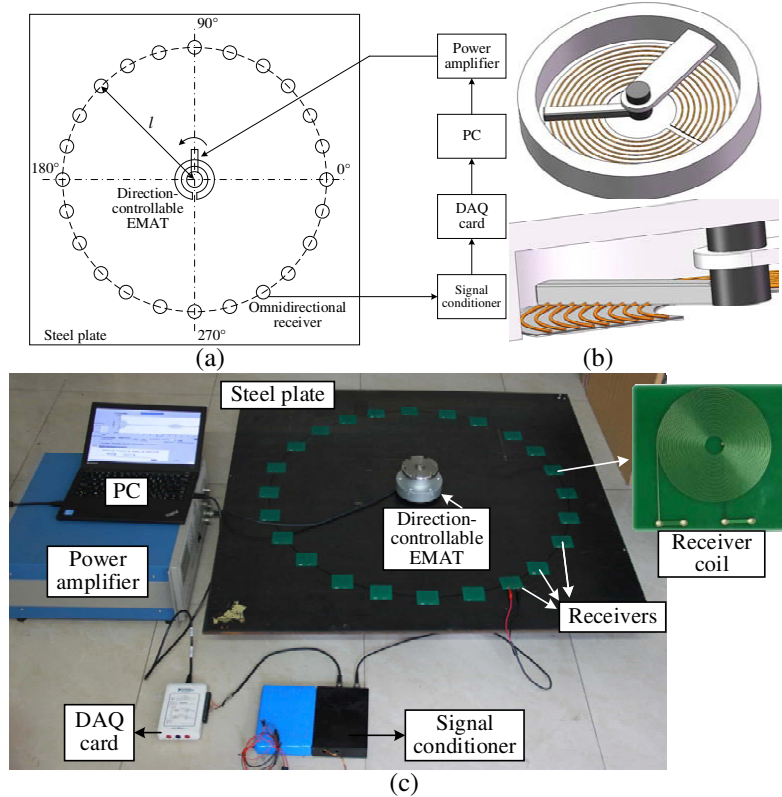


Figure 6. The setup of the experimental system. (a) The layout of transducers and the schematic diagram, (b) the inner structure of the direction-controllable EMAT, (c) the photo of the experimental system.

The direction-controllable EMAT is installed on the 4 mm thick steel plate, and the current coils are excited by the power amplifier, whose parameters such as the excitation voltage, frequency and number of cycles are controlled by the PC. The excitation voltage is 80 V, the number of cycles 10, and the working frequency 320 kHz. According to the previously defined dead zone angle of the EMAT and the preset angle coordinate system, the working angles that the EMAT can cover are from 284.37° to 255.63° , rotating anticlockwise. Totally 24 omnidirectional receivers [25] are uniformly distributed along the circumference centered at the direction-controllable EMAT, and the radius angle between any two receivers is 15° . The racetrack coil is employed in the typical omnidirectional receiver, as shown in Fig. 6(c). The diameter of the receiver coil is 35 mm, and there are 30 turns of windings in the receiver to obtain relatively larger signal amplitude. And the dimension of the receiver is small enough for 30 turns of windings to try to eliminate the influence of receiver's dimension on the performance of the direction-controllable EMAT. The distance from the direction-controllable EMAT to any of the receivers is l . The receivers convert the received SH0 mode waves into electrical signals, and then the signals are amplified and filtered by the signal conditioner. Then the detection signals are acquired by the data acquisition card, and finally the detection data are transferred to the PC to be processed and analyzed.

Detection data that are transferred to the PC can be represented as $x(n)$, $n = 1, 2, \dots, N$, where N is the total number of the detection data points. In order to evaluate the strength of the received

SH waves, the power of the detection data is defined as

$$p = \frac{1}{N} \sum_{n=1}^N |x(n)|^2 \quad (4)$$

Firstly, the directionality and the focus level are studied about the direction-controllable EMAT. The direction rotary knob is rotated to be at the position 90° , and the distance between the direction-controllable EMAT and receivers is $l_1 = 0.5$ m. The waveforms from the receiver at 90° is shown in Fig. 7(a). The first waveform is the initial pulse signal from space by the excitation current, and the second waveform is the received SH0 wave. Detection data from each receiver are transferred to the PC, and the power of each received detection data is calculated. The normalized power distribution of the detection data from each receiver is illustrated in Fig. 7(b).

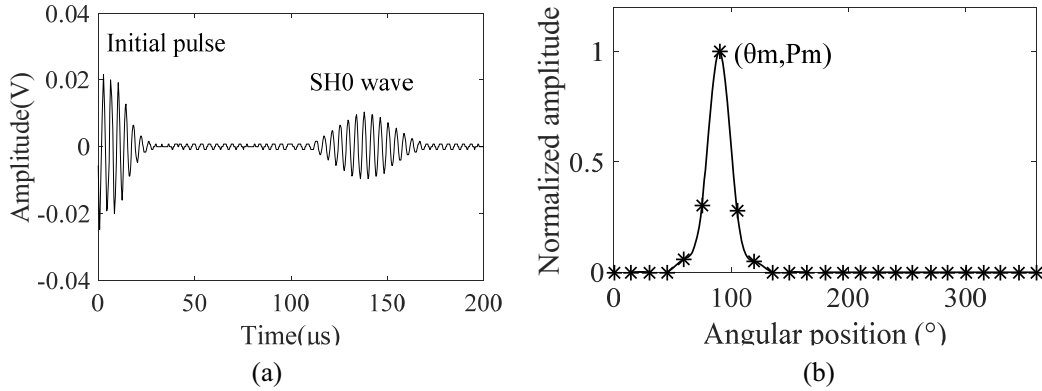


Figure 7. The experiment result at 90° , (a) the waveforms from the receiver at 90° , (b) the normalized power distribution of all the detection data.

It is indicated in Fig. 7(b) that most of the signal power is focused in the area around 90° of the angular position, and it corresponds to the receiver that directly faces the stimulation direction of the new EMAT. The angular position is represented as θ here, and the point with maximum signal power is (θ_m, p_m) . The power threshold p_t is defined here as

$$p_t = a * p_m \quad (5)$$

where a is the power threshold factor, and it satisfies $0 < a < 0.5$. The definition of the power threshold helps to evaluate the focus level of the directionality.

The angular thresholds are respectively defined as

$$\theta_{t1} = \arg \min |p(\theta) - p_t| \cap (\theta < \theta_m) \quad (6)$$

$$\theta_{t2} = \arg \min |p(\theta) - p_t| \cap (\theta > \theta_m) \quad (7)$$

The focus angle θ_f is defined to describe that most power of the stimulated SH0 mode waves is situated in this angle range:

$$\theta_f = \theta_{t2} - \theta_{t1} \quad (8)$$

In this specific experiment where the angular position is 90° , the power threshold factor is set as 0.2, and the calculated angular thresholds are 72.5° and 107° . Therefore, the focus angle at this experiment situation is 34.5° .

Besides, the directionality and focus level may vary with the distance between the receivers and the new EMAT. The distance can be increased to l_2 to satisfy

$$p_m(l_2) < b * p_m(l_1) \quad (9)$$

where b is the comparing factor to guarantee that the distance l_2 is far enough, and the amplitude of the signal is fairly small. In this situation, the focus angle θ_f can be calculated as

$$\theta_f = \min \left\{ \frac{l_1}{l_2} \theta_{f1}, \theta_{f2} \right\} \quad (10)$$

Further experiment is conducted with $l_2 = 1.5$ m, and the calculated θ_{f2} is 10.7° . Therefore, the focus angle considering the distance between the direction-controllable EMAT and receivers is 10.7° .

Secondly, the circumferential consistency is considered about the direction-controllable EMAT. Except for the dead zone of the EMAT, the direction rotary knob is rotated from 284.37° to 255.63° , with 15° as the step. Therefore, totally 23 receivers, except for the one at angular position 270° , will respectively and directly face the direction of the rotary knob and receive the coming SH0 mode waves. The power of detection data from each receiver at each angular position is calculated. Fig. 8 shows the normalized power of each receiver.

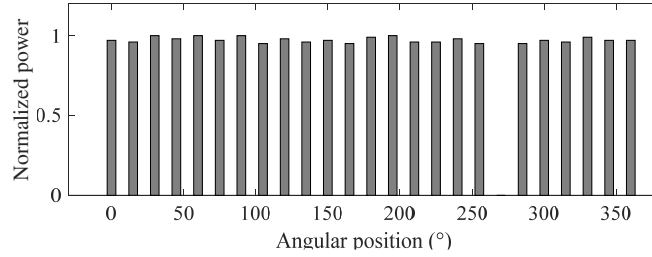


Figure 8. The normalized power of each receiver for the circumferential consistency experiment.

It is indicated in Fig. 8 that the direction-controllable EMAT owns a fairly good consistency on the circumferential working angles. In order to quantify the circumferential consistency, the consistency error E_c is defined

$$E_c = \frac{1}{M} \sum_{m=1}^M |p(m) - p_E| \quad (11)$$

$$p_E = \frac{1}{M} \sum_{m=1}^M p(m) \quad (12)$$

where M is the total number of the valid receivers, except for the one at angular position 270° , so $M = 23$. And the calculated consistency error E_c is 1.4%, which indicates a relatively small inconsistency for the working directions of the direction-controllable EMAT.

Besides, in the circumferential consistency experiment based on the experimental system in Fig. 6, the receiver at position 270° is in the dead zone, and its two adjacent receivers are out of the dead zone, but they are quite close. The central angle between the two adjacent receivers is 30° , which is bigger than the dead zone angle 28.74° . Results in Fig. 8 illustrate that the two adjacent receivers can normally receive guided waves while the receiver at position 270° cannot. This verifies that the dead zone angle is less than 30° , which shows a good agreement with the physical definition of the dead zone.

5. CONCLUSIONS

This work proposes a novel direction-controllable EMAT for SH0 waves in steel plate based on magnetostriction. The technique background and practical requirement for direction-controllable EMAT are demonstrated. SH0 mode wave does not suffer from dispersion, and it is selected as the desired mode GW for the new EMAT. Theoretical analysis about the magnetostriction model of EMAT and working parameters determination are conducted. Then the detailed structure and design of the direction-controllable EMAT are presented. The pre-magnetized open annular nickel strap is bonded to the steel plate to provide the circumferential static bias magnetic field. The dynamic magnetic field is provided by the cooperation of embedded conductors in the rotating slider and the open metal rings.

The experimental system for the performance verification of the new EMAT is set up. The dead zone angle, focus angle and consistency error of the new EMAT are defined to evaluate the performance quantitatively. Besides, the direction and focus level experiment and the circumferential consistency experiment are conducted based on the experimental platform. The dead zone angle of the new

EMAT is 28.74° , the focus angle 10.7° , and the consistency error only 1.4%. Results show that the proposed direction-controllable EMAT is highly directional. The stimulating direction can be accurately controlled, and the circumferential consistency is fairly high. This direction-controllable EMAT can hopefully provide a practical and promising solution for directional monitoring and inspecting for steel plate structures.

ACKNOWLEDGMENT

This research was supported by the National Natural Science Foundation of China (NSFC) (No. 51277101), the Royal Society-NSFC International Exchanges Award (No. IE150600), the Royal Academy of Engineering Newton Research Collaboration Program (No. NRCP/1415/91) and the Royal Academy of Engineering Distinguished Visiting Fellowship program (No. DVF1415/2/17).

REFERENCES

1. Zhao, Q., J. N. Hao, and W. L. Yin, "A simulation study of flaw detection for rail sections based on high frequency magnetic induction sensing using the boundary element method," *Progress In Electromagnetics Research*, Vol. 141, 309–325, 2013.
2. Shlivinski, A., "Ultra wideband wave-based linear inversion in lossless ladder networks," *Progress In Electromagnetics Research*, Vol. 125, 97–118, 2012.
3. Gravenkamp, H., "A remark on the computation of shear-horizontal and torsional modes in elastic waveguides," *Ultrasonics*, Vol. 69, 25–28, 2016.
4. Wang, Q., M. Hong, and Z. Q. Su, "An in-situ structural health diagnosis technique and its realization via a modularized system," *IEEE Transactions on Instrumentation and Measurement*, Vol. 64, 873–887, 2015.
5. Li, J. and B. Shanker, "Time-dependent Lorentz-Mie-Debye formulation for electromagnetic scattering from dielectric spheres," *Progress In Electromagnetics Research*, Vol. 154, 195–208, 2015.
6. Lee, J., J. Park, and Y. Cho, "A novel ultrasonic NDE for shrink fit welded structures using interface waves," *Ultrasonics*, Vol. 68, 1–7, 2016.
7. Hirao, M. and H. Ogi, "An SH-wave EMAT technique for gas pipeline inspection," *NDT & E International*, Vol. 32, 127–132, 1999.
8. Khalili, P. and P. Cawley, "Excitation of single-mode lamb waves at high-frequency-thickness products," *IEEE Transactions on Ultrasonics Ferroelectrics and Frequency Control*, Vol. 63, 303–312, 2016.
9. Karaikos, G., A. Deraemaeker, D. G. Aggelis, and D. Van Hemelrijck, "Monitoring of concrete structures using the ultrasonic pulse velocity method," *Smart Materials and Structures*, Vol. 24, 113001, 2015.
10. Murayama, R., "Non-destructive evaluation of formability in cold rolled steel sheets using the SH0-mode plate wave by electromagnetic acoustic transducer," *Ultrasonics*, Vol. 39, 335–343, 2001.
11. Ding, J. C., B. Wu, and C. F. He, "Reflection and transmission coefficients of the SH0 mode in the adhesive structures with imperfect interface," *Ultrasonics*, Vol. 70, 248–257, 2016.
12. Lowe, P. S., R. M. Sanderson, N. V. Boulgouris, A. G. Haig, and W. Balachandran, "Inspection of cylindrical structures using the first longitudinal guided wave mode in isolation for higher flaw sensitivity," *IEEE Sensors Journal*, Vol. 16, 706–714, 2016.
13. Glushkov, E., N. Glushkova, A. Eremin, and R. Lammering, "Group velocity of cylindrical guided waves in anisotropic laminate composites," *Journal of the Acoustical Society of America*, Vol. 135, 148–154, 2014.
14. Keller, S. M., A. E. Sepulveda, and G. P. Carman, "Effective magnetoelectric properties of magnetoelectroelastic (multiferroic) materials and effects on plane wave dynamics," *Progress In Electromagnetics Research*, Vol. 154, 115–126, 2015.
15. Thring, C. B., Y. Fan, and R. S. Edwards, "Focused Rayleigh wave EMAT for characterisation of surface-breaking defects," *NDT & E International*, Vol. 81, 20–27, 2016.

16. Seher, M. and R. Challis, "The electrical properties of a planar coil electromagnetic acoustic transducer and their implications for noise performance," *Measurement Science and Technology*, Vol. 27, 025102, 2016.
17. Lee, J. K., H. W. Kim, and Y. Y. Kim, "Omnidirectional lamb waves by axisymmetrically-configured magnetostrictive patch transducer," *IEEE Transactions on Ultrasonics Ferroelectrics and Frequency Control*, Vol. 60, 1928–1934, 2013.
18. Ribichini, R., F. Cegla, P. B. Nagy, and P. Cawley, "Experimental and numerical evaluation of electromagnetic acoustic transducer performance on steel materials," *NDT & E International*, Vol. 45, 32–38, 2012.
19. Dixon, S., M. P. Fletcher, and G. Rowlands, "The accuracy of acoustic birefringence shear wave measurements in sheet metal," *Journal of Applied Physics*, Vol. 104, 114901, 2008.
20. Seung, H. M., C. Il Park, and Y. Y. Kim, "An omnidirectional shear-horizontal guided wave EMAT for a metallic plate," *Ultrasonics*, Vol. 69, 58–66, 2016.
21. Wilcox, P. D., M. Lowe, and P. Cawley, "Omnidirectional guided wave inspection of large metallic plate structures using an EMAT array," *Ieee Transactions on Ultrasonics Ferroelectrics and Frequency Control*, Vol. 52, 653–665, 2005.
22. Roh, Y. and J. Kim, "Detection of cracks on a plate by piezoelectric interdigital transducers," *Sensors and Smart Structures Technologies for Civil, Mechanical, and Aerospace Systems*, 2011.
23. Masuyama, H., K. Mizutani, and K. Nagai, "Sound source with direction-variable beam using annular transducer array," *2002 IEEE Ultrasonics Symposium Proceedings*, Vols. 1–2, 1097–1100, 2002.
24. Iwaya, K., R. Murayama, and T. Hirayama, "Study of ultrasonic sensor that is effective for all direction using an electromagnetic force," *International Conference on Experimental Mechanics 2014*, Vol. 9302, 2015.
25. Wei, Z., S. L. Huang, S. Wang, and W. Zhao, "Magnetostriction-based omni-directional guided wave transducer for high-accuracy tomography of steel plate defects," *IEEE Sensors Journal*, Vol. 15, 6549–6558, 2015.